Available online at www.sciencedirect.com
ScienceDirect
Journal of Sound and Vibration 302 (2007) 875–891
JOURNAL OF SOUND AND VIBRATION
www.elsevier.com/locate/jsvi

Structural vibration control using linear magnetostrictive actuators

Seok-Jun Moon[a,*], Chae-Wook Lim[b], Byung-Hyun Kim[a], Youngjin Park[c]

[a]*Korea Institute of Machinery & Materials, 171 Jang-dong, Yuseong, Daejeon, 305-343, Republic of Korea*
[b]*Doosan Heavy Industries & Construction CO., Ltd., Yuseong, Daejeon, 305-348, Republic of Korea*
[c]*Korea Advanced Institute of Science & Technology, Science Town, Daejeon, 305-701, Republic of Korea*

Received 1 November 2006; accepted 15 December 2006
Available online 16 February 2007

Abstract

Terfenol-D is one of several magnetostrictive materials with the property of converting energy into mechanical motion, and vice versa. We designed and fabricated a linear magnetostrictive actuator (MSA) using Terfenol-D as a control device. In order to grasp the dynamic characteristics of the actuator, a series of experimental and numerical tests were performed. Induced-strain actuation displacements of the actuator measured by the test and predicted by magnetic analysis agreed well, and blocked forces, according to the input currents, were estimated from the testing results. A modeling method representing the exerting force of the actuator was confirmed through some testing results. We also explored the effectiveness of the linear MSA as a structural control device. A series of numerical and experimental tests was carried out with a simple aluminum beam supported only at each end by such an actuator. After the equation of motion of the controlled system was obtained by the finite element method, a model reduction was performed to reduce the number of degrees of freedom. A linear quadratic feedback controller was implemented on a real-time digital control system to dampen the first four elastic modes of the beam. Through some tests, we confirmed the capability of the actuator for controlling beam-like structures.

1. Introduction

Actuators based on the piezoelectric effect are suitable for active vibration control because of their wide frequency range and relatively high actuation forces. Two types of piezoelectric actuators are commonly used. Piezoelectric patches applied on a simple mechanical structure have proved to be very effective in vibration control. But the location of the commonly used piezo patches, which are bonded on or integrated in the structure, is an important issue. The use of piezoelectric stack actuators helps to avoid these advantages. Stack actuators are mainly employed in the control of large space structures like satellites. Maertens and Waller [1] have investigated the active vibration control of an aluminum plate with piezoelectric stack actuators.

*Corresponding author. Tel.: +82 42 868 7428; fax: +82 42 868 7418.
E-mail address: sjmoon@kimm.re.kr (S.-J. Moon).

0022-460X/$ - see front matter © 2007 Elsevier Ltd. All rights reserved.
doi:10.1016/j.jsv.2006.12.023

As another stack-type actuator, the magnetostrictive actuator (MSA) is in the limelight using a giant magnetostrictive material such as Terfenol-D. Terfenol-D can produce great forces; fast, high-precision motion; high efficiencies; and high power levels [2]. This material has other notable properties, which are of practical value, these include [3]:

- a high magnetomechanical coupling, enabling the efficient conversion of magnetic to mechanical energy,
- a high load bearing capability,
- high compressional strength,
- durability under static and dynamic loading,
- low voltage operation, and
- high reliability and unlimited life cycle [4].

Therefore, research on MSA has recently been undertaken in many application fields. During the European Commission funded project MADAVIC (Magnetostrictive Actuators for Damage Analysis and Vibration Control), six actuator prototypes have been developed [5,6]. Maier and Seesmann [7] have characterized the dynamic behavior of an MSA and developed two analytical models based on linear constitutive equations. Moreover, a control scheme for the MSA has been presented, which not only stabilized the mathematical model of the magnetostrictive rod, but also led to an excellent tracking behavior [8]. Zhang et al. [9] have developed giant MSAs for active vibration control, performed some experiments, and achieved better vibration attenuation results.

In this research, a linear MSA using Terfenol-D has been designed and fabricated as a control device. A series of experimental and numerical tests have been performed to grasp the dynamic characteristics of the actuator. The induced-strain displacement of the linear MSA has been measured and predicted by magnetic analysis, and blocked force, according to the input currents, has been estimated from the testing results. The effectiveness of the linear MSA as a structural control device has also been explored. A series of numerical and experimental tests have been carried out with simple aluminum beam supported only at each end by such actuators. A linear quadratic feedback controller has been implemented on a real-time digital control system to dampen the first four elastic modes of the beam. Through some tests, the capability of the linear MSA for structural control has been confirmed.

2. Design and fabrication of an MSA

Terfenol-D is an alloy of terbium, dysprosium, and iron metals. In technical terms, Terfenol-D is a solid-state transducer capable of converting very high energy levels from one form to another. In the case of electrical-to-mechanical conversion, the magnetostriction of the material generates strains 20 times greater than traditional magnetostrictives, and 2–5 times greater than traditional piezoceramics.

In this research, the $Tb_{0.3}Dy_{0.7}Fe_{1.9}$ Terfenol-D produced by ETREMA Products, Inc. [10] is used. Physical properties of the Terfenol-D are summarized in Table 1. A linear MSA is conceptually designed as shown in

Table 1
Physical properties of Terfenol-D [10]

Item	Property	Item	Property
Mechanical property	• Young's modulus: 25–35 GPa • Compressive strength: 700 MPa • Tensile strength: 28 MPa • Sound speed: 1640–1940 m/s	Electrical property	• Resistivity: 58 μΩ cm • Curie temperature: 380 °C
Magnetostrictive property	• Maximum strain: 1000–2000 ppm • Strain estimated linear: 800–1200 ppm • Energy density: 14–25 kJ/m^2	Magnetomechanical property	• Relative permeability: 3–10 • Coupling factor: 0.75

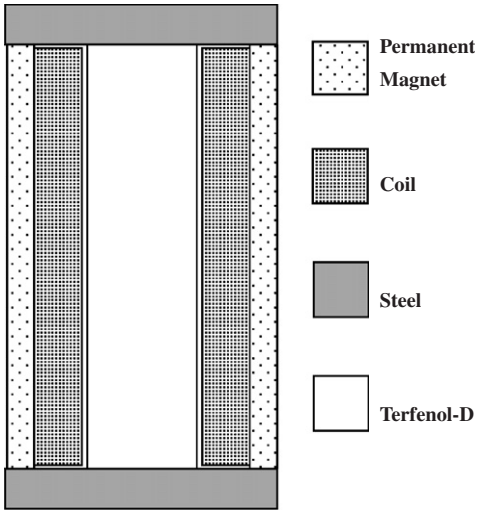

Fig. 1. Conceptual design of linear magnetostrictive actuator.

Fig. 1. The linear MSA consists of a Terfenol-D rod inside an electric coil for generating magnetic field and enclosed by an annular permanent magnet for magnetic bias. The Terfenol-D rod, the coil, and the magnet are assembled between two steel-washers (end plates). A commercial magnetostrictive rod with 25 mm in diameter and 100 mm long is selected. In order to design the MSA in detail, some parameters such as prestress level, magnetic bias, coil size, and so on must be determined. The magnetostriction S of Terfenol-D is a function of mechanical compressive prestress T_p, magnetic field intensity H, and temperature t [11]. The room-temperature magnetostriction of the Terfenol-D rod is experimentally obtained as a function of magnetic field intensity for different prestress levels as shown in Fig. 2. Maximum magnetostriction occurs at prestress level of 7 MPa and its curve has a nearly linear section. So, prestress level of 7 MPa is determined. This value is realized using a specific spring with stiffness of 324 kN/m. Regardless of magnetic field polarity, Terfenol-D can provide only positive strain. To obtain both positive and negative strains, magnetic biasing H_b is required. This biasing effect may be provided by permanent magnets, thus minimizing the need for electrical bias current and so reducing power requirements. The bias magnetization level of about 20 kA/m is properly considered from Fig. 2. A solenoid coil is wound around the rod to expand or contract in response, leading to proportional, positive, and repeatable expansion in either positive or negative magnetic field direction. A nonlinear magnetic field analysis, using a finite element method, is carried out to decide the coil turns, thickness of permanent magnets and end plates, and so on. Figs. 3 and 4 show the typical magnetic field intensities in Terfenol-D rod induced by ferrite permanent magnets and by coils, respectively.

The actuator displacement under zero external load is commonly known as "free stroke". Measurement of the actuator free stroke gives the value of the induced-strain actuator displacement, u_{ISA} [12]. The value is one of the overall performance parameters of various solid-state actuators. Therefore, u_{ISA} of the designed MSA is theoretically predicted using simple linear magnetic field analysis. The magnetic path induced by a coil and working current can be assumed as shown in Fig. 5. The path consists of two loops; inner loop with the Terfenol-D rod, end plates and permanent magnets; and outer loop with end plates and air. Every parameter denoted in Fig. 5 is defined in the following equation:

$$\begin{aligned} &l_T = l_4, \quad l_1 = l_3 = l_5 = l_{10} = w_h/2, \quad l_2 = l_9 = d_T/2 + w_c + w_p/2, \\ &l_6 = l_8 = w_p/2, \quad l_7 = \pi(l_3 + l_4 + l_5)/2, \end{aligned} \tag{1}$$

where thickness of the end plate is $w_h = 8$ mm, thickness of the permanent magnet $w_p = 11$ mm, thickness of the coil $w_c = 12$ mm, diameter of the rod $d_T = 25$ mm, and length of the rod $l_T = 100$ mm. An equivalent magnetic circuit can replace the magnetic path in Fig. 5 using electric items. In Fig. 6, N and I represent coil

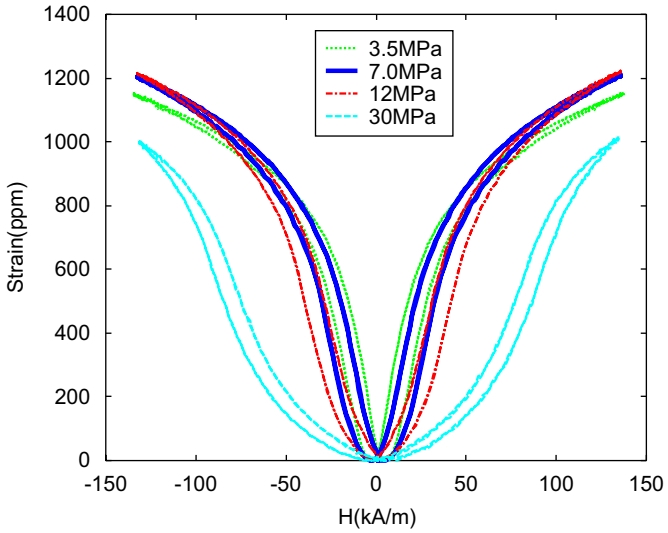

Fig. 2. Magnetostriction versus magnetic field intensity.

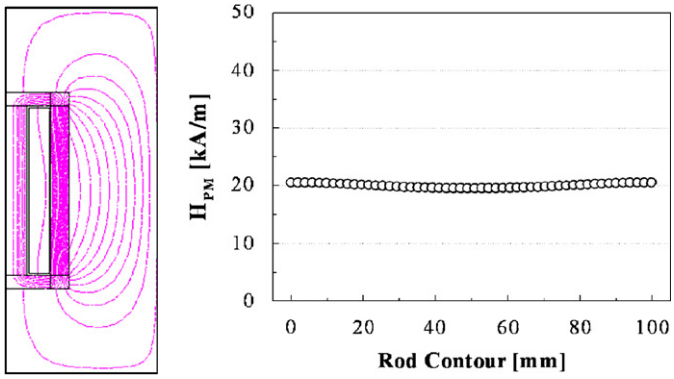

Fig. 3. Magnetic field intensity in Terfenol-D rod induced by a permanent magnet.

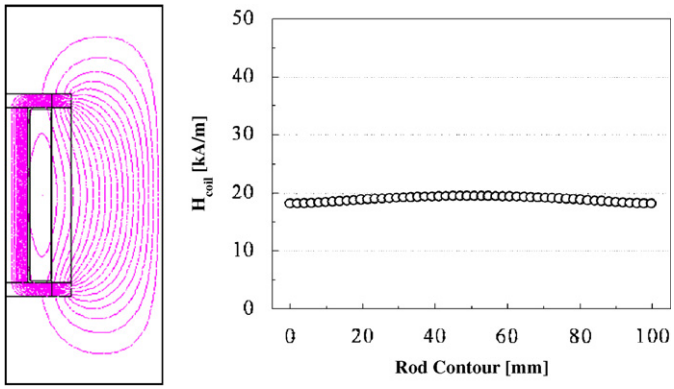

Fig. 4. Magnetic field intensity in Terfenol-D rod induced by a coil.

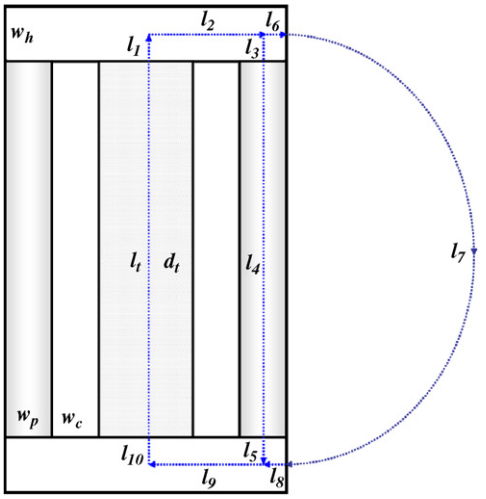

Fig. 5. Magnetic path induced by a coil.

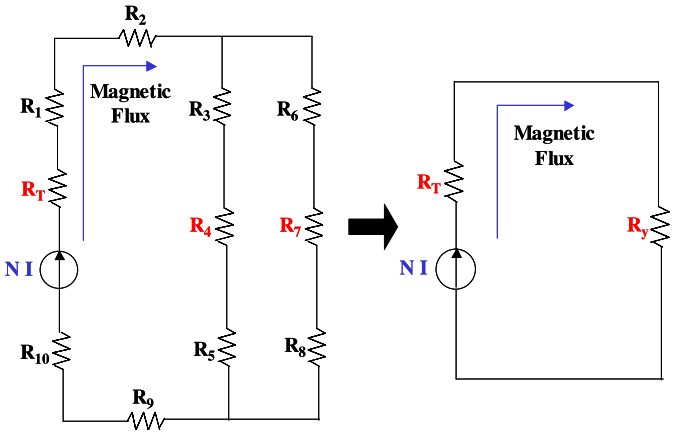

Fig. 6. Equivalent magnetic circuit.

turns and input current, respectively, and equivalent resistances may be obtained from the following equation:

$$R_i = \frac{l_i}{\mu_i A_i} \tag{2}$$

where μ_i is the magnet permeability, and A_i is the equivalent area which is expressed as

$$\begin{aligned} &A_t = A_1 = A_{10} = \pi d_T^2/4, \quad A_2 = A_9 = \pi w_h l_2, \quad A_3 = A_4 = A_5 = 4\pi l_2 l_6, \\ &A_6 = A_8 = \pi w_h(2l_2 + l_6), \quad A_7 = \pi(l_2 + l_6)(r_b - r_a) + 2(r_b^2 - r_a^2), \\ &r_a = l_4/2 - w_p, \quad r_b = l_4/2 + w_h + w_p. \end{aligned} \tag{3}$$

Assuming that there is no magnetic loss, Maxwell's equation can be expressed in the following terms:

$$NI = \oint \vec{H}\,\mathrm{d}\vec{x} = H_T l_T + R_y A_T \mu_T H_T, \tag{4}$$

Fig. 7. Fabricated linear magnetostrictive actuator.

where H_T, A_T, and μ_T represent magnetic field intensity in the rod, sectional area of the rod, and magnet permeability of the rod, respectively. Therefore, H_T can be calculated from the following equation:

$$H_T = \frac{u_{\mathrm{ISA}}}{c_b l_T}, \tag{5}$$

where u_{ISA} is induced-strain actuation displacement and c_b is the slope at the magnetic biasing point H_b in Fig. 1. From Eqs. (4) and (5), u_{ISA} can be obtained:

$$\frac{u_{\mathrm{ISA}}}{I} = \frac{c_b N l_T}{l_T + R_y A_T \mu_T}. \tag{6}$$

The u_{ISA} per current is predicted to have 9.57 μm/A from Eq. (6).

Through these investigations, it is decided that ferrite permanent magnet has a thickness of 11 mm, coil 1.0 mm in diameter and 700 turns at working current of 5.0 A, and steel plates 8 mm in thickness. Based on the analysis results, the linear MSA is fabricated as shown in Fig. 7.

3. Identification of dynamic characteristics

The displacement characteristics of the fabricated linear MSA are investigated through experimental tests. Fig. 8 shows the experimental setup for measuring the induced-strain actuator displacement, u_{ISA}. The MSA is fully fixed on the rigid structure and a non-contact gap sensor is mounted to measure the tip displacement as shown in Fig. 8. For direct current (DC) input at intervals of 0.5 A, the u_{ISA} measured is shown in Fig. 9. The results say that the u_{ISA} to the input current has nearly linear characteristics with slope of 9.17 μm/A up to 3 A.

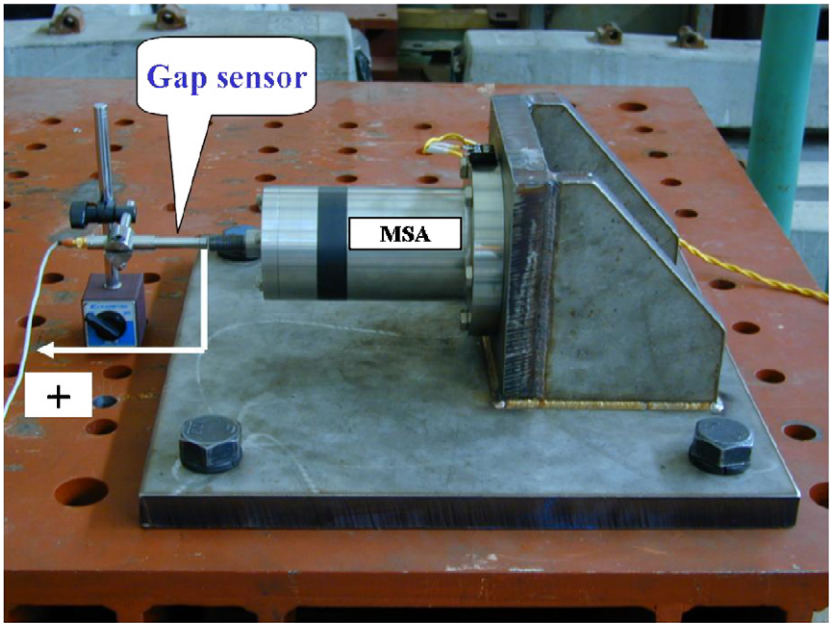

Fig. 8. Experimental setup for displacement measurement.

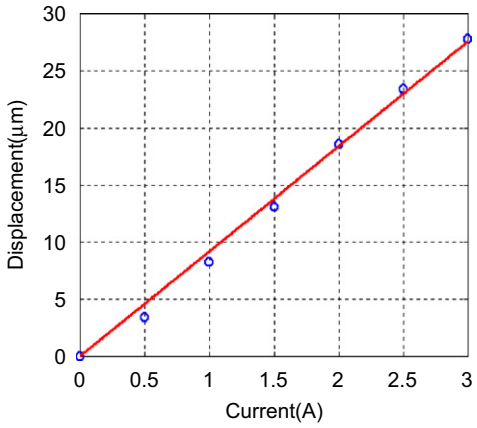

Fig. 9. Induced-strain actuator displacement of the MSA under DC diving conditions.

This value agrees well with the theoretically predicted value (9.57 μm/A) in Section 2. The MSA makes the induced strain of Terfenol-D to be only about 550 ppm in linear range. It is less than the linear range of 800–1200 ppm shown in Table 1. To improve the linear range of the induced strain of the Terfenol-D, it is recommended that Terfenol-D having strain properties longer than that used in ours be used.

Next, while alternating current (AC) with intervals of 5 Hz is applied, the displacement responses are measured. Through the results shown in Fig. 10, it is confirmed that the u_{ISA} has constant displacement characteristics within the range of current frequency measured.

Since the maximum force of the MSA is realized when the actuator is fully blocked, the force characteristics of the MSA may be expressed by blocked force [12]. In order to measure the blocked force directly, the stiffness of external blocking fixture must be infinite. Because, the fixture cannot have an infinite stiffness, the blocked force of the MSA should be indirectly predicted from dynamic testing results. As shown in Fig. 11, the MSA is fixed using steel fixtures at both ends. A gap sensor and a piezoelectric-type force transducer are

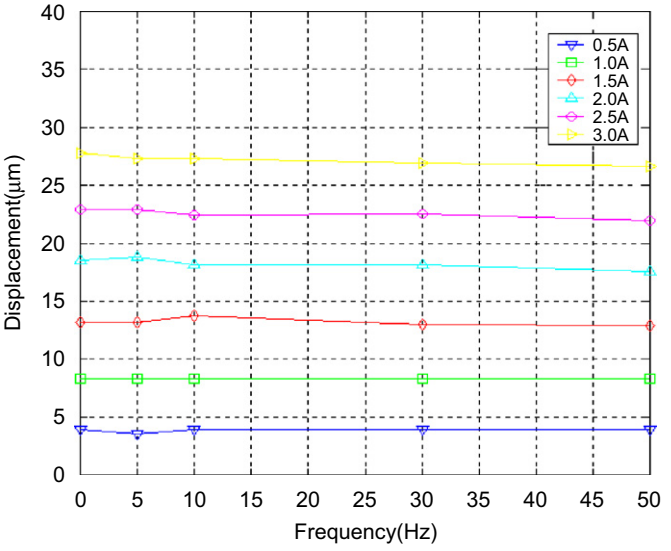

Fig. 10. Induced-strain actuator displacements of the MSA under AC diving conditions.

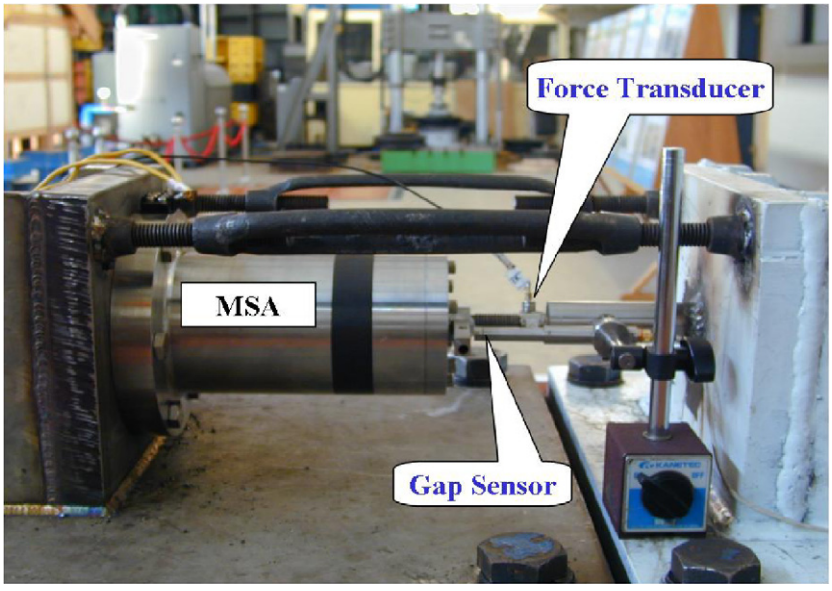

Fig. 11. Experimental setup for force measurement.

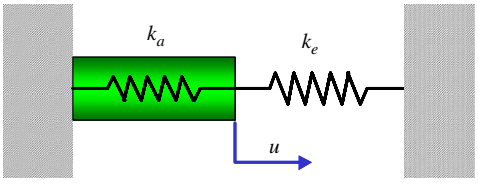

Fig. 12. Schematic diagram of the MSA with flexible structure.

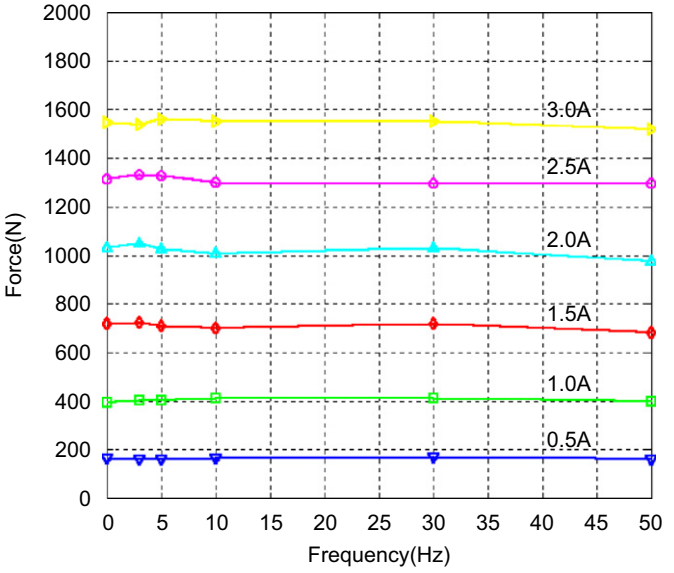

Fig. 13. Force responses under AC diving conditions.

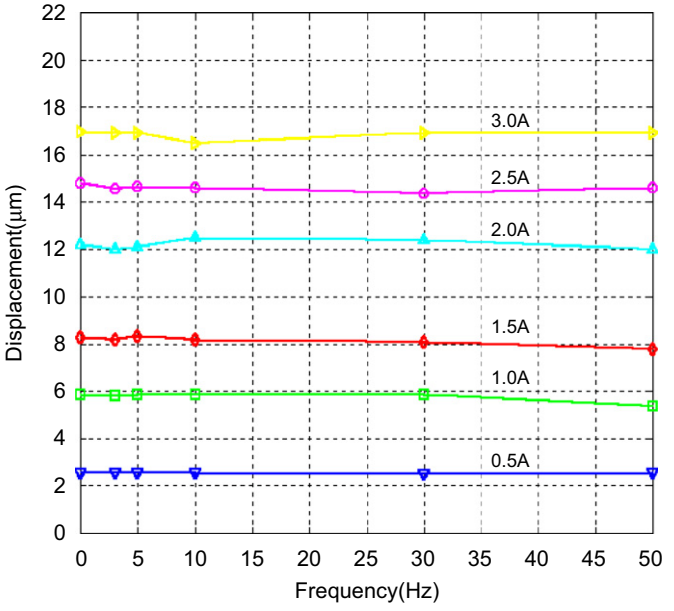

Fig. 14. Displacement responses under AC diving conditions.

installed to measure the responses. The MSA can be modeled as shown in Fig. 12 using internal stiffness of the MSA, k_a, external stiffness of the fixture, k_e, and displacement u. Because k_e is not infinite, u exists in the range of $0<u<u_{\mathrm{ISA}}$. When the current is input from 0 to 3 A, force F_a and displacement u of the MSA are measured. Figs. 13 and 14 show the results under alternating current up to 50 Hz. It is confirmed that they have nearly linear characteristics with respect to input current and flat characteristics with respect to frequency. As an example, Fig. 15 shows the measured time histories of the driving voltage, input current, displacement, and force at 1.5 A and 10 Hz.

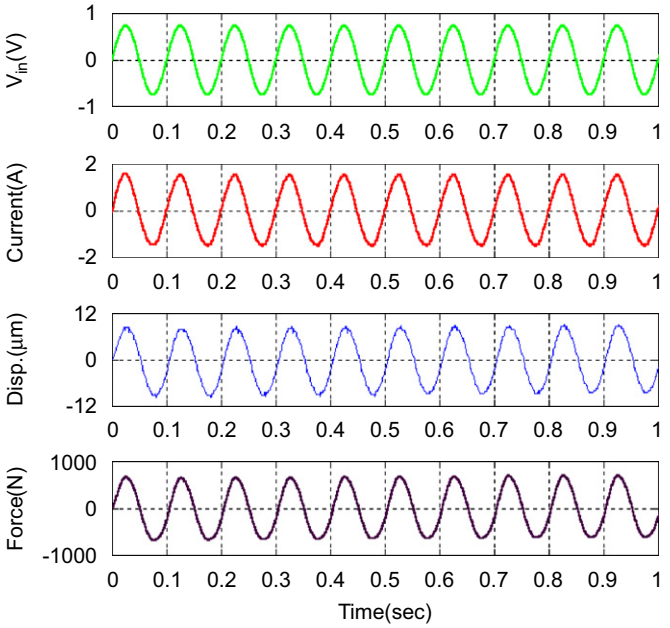

Fig. 15. Time histories of the measured data for 1.5 A at 10 Hz.

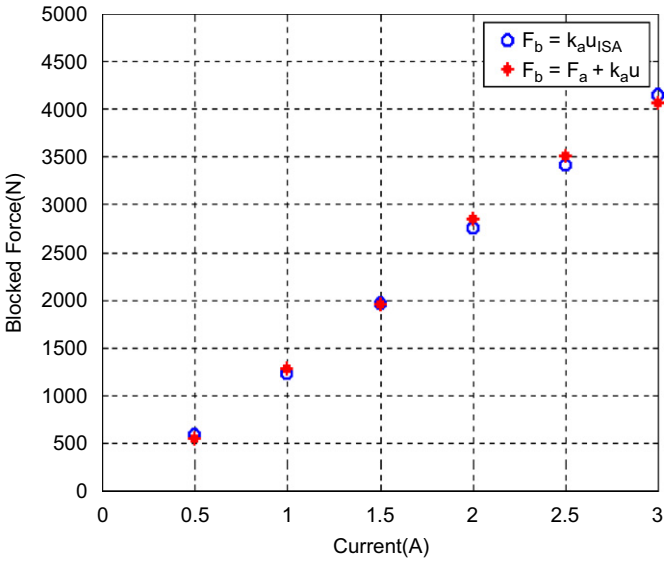

Fig. 16. Comparison of the blocked forces.

The blocked force of the MSA can be mathematically defined by

$$F_b = k_a u_{\mathrm{ISA}}, \tag{7}$$

where k_a is the blocked force, which cannot be measured. However, the blocked force may be predicted from measured responses from the following equation:

$$F_b = F_a + k_a u, \tag{8}$$

where $k_a = A_T E_T / l_T = 149.21$ MN/m. In order to verify the accuracy of Eq. (8), the predicted blocked force is compared with calculated force from Eq. (7). Fig. 16 shows the result. Since the two blocked forces are agreed

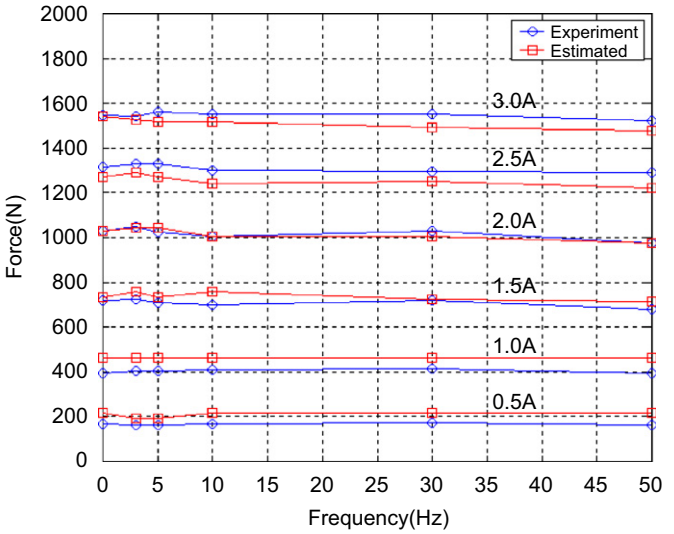

Fig. 17. Experiment versus estimation of force.

well, the blocked force of the MSA is accurately predicted from Eq. (8). On the other hand, force F_a can be expressed by

$$F_a = k_e u. \tag{9}$$

Substituting Eqs. (7) and (9) into Eq. (8), the displacement of the MSA can be obtained from

$$u = \frac{u_{\mathrm{ISA}}}{1 + k_e/k_a} \tag{10}$$

and substituting Eq. (10) into Eq. (9), the force of the MSA can be obtained from

$$F_a = k_e \frac{u_{\mathrm{ISA}}}{1 + k_e/k_a}. \tag{11}$$

The force estimated from Eq. (11) is compared with the measured data in Fig. 17. The figure shows the comparison of the dynamic forces with flexible support with respect to input current and frequency. Although there is a little error, the results are considered acceptable. Thus, the displacement and force of the fabricated MSA can be predicted using Eqs. (10) and (11).

4. Application: active vibration control

The developed MSA is applied to vibration control as a control device. In order to check the effectiveness and capability of the linear MSA, the experiment and numerical simulation regarding active vibration control are carried out on a simple beam. An aluminum beam is simply supported at each end by the MSA as shown in Fig. 18. The beam is 1000 mm (L) long, 25 mm (b) wide, and 10 mm (h) high. The specific jig is used to achieve simply supporting conditions at the ends. In case the MSA is connected with a flexible structure modeled with a lumped mass and a spring, the system may be equivalently modeled as shown in Fig. 19. In Fig. 19, m and k_e denote mass and stiffness of the structure connected to the MSA. The generated force from the MSA is

$$F_a = k_a(u_{\mathrm{ISA}} - u) \tag{12}$$

and the equation of motion of the structure is

$$F_a = m\ddot{u} + k_e u. \tag{13}$$

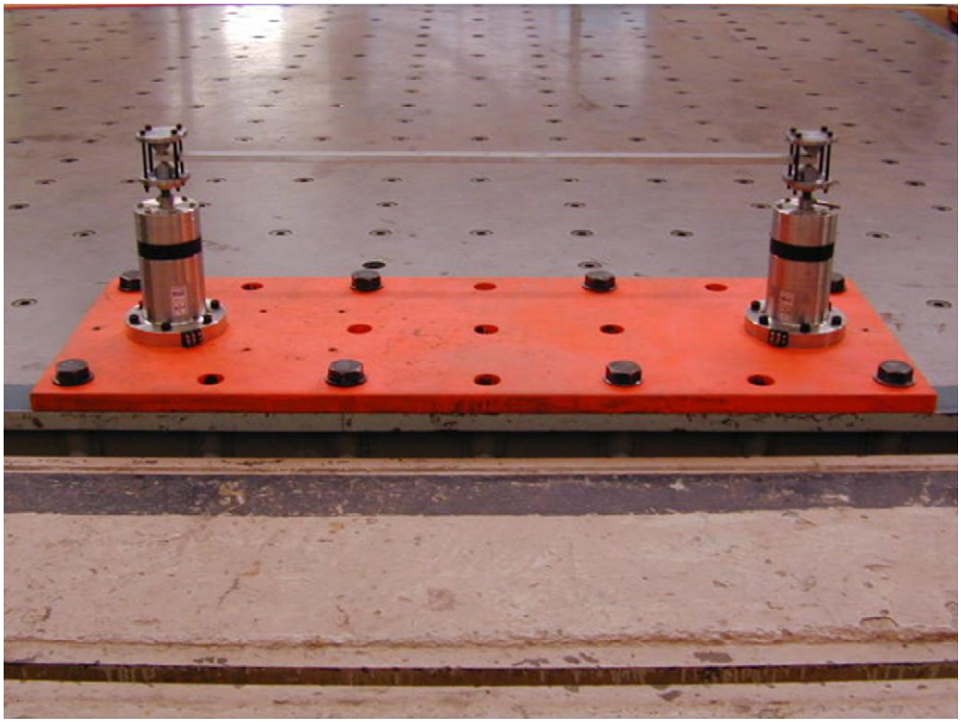

Fig. 18. Overview of the experimental setup for active vibration control.

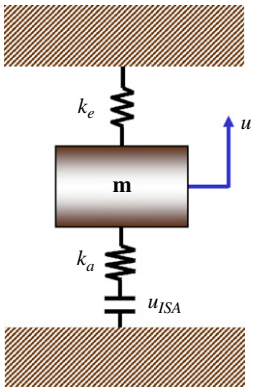

Fig. 19. Equivalent mathematical model.

From Eqs. (12) and (13), the following equation is obtained:

$$m\ddot{u} + (k_e + k_a)u = k_a u_{\mathrm{ISA}}. \tag{14}$$

Since u_{ISA} and k_a of the MSA are known parameters, the dynamic responses of the structure are calculated based on Eq. (14).

For the numerical simulation and experiment of the active control system, the equation of motion of the test structure is first obtained. The test structure in Fig. 18 is modeled using 10 beam elements as shown in Fig. 20. The boundary condition at each end is expressed by the stiffness of the MSA. Using static condensation method, the equation of motion is formulated. Displacements in rotational direction are removed. Because of the finite stiffness of the actuator at each end, the displacement response can occur at each end. The first four natural frequencies of the test structure are summarized in Table 2. In case both u_1 and u_2 have the same

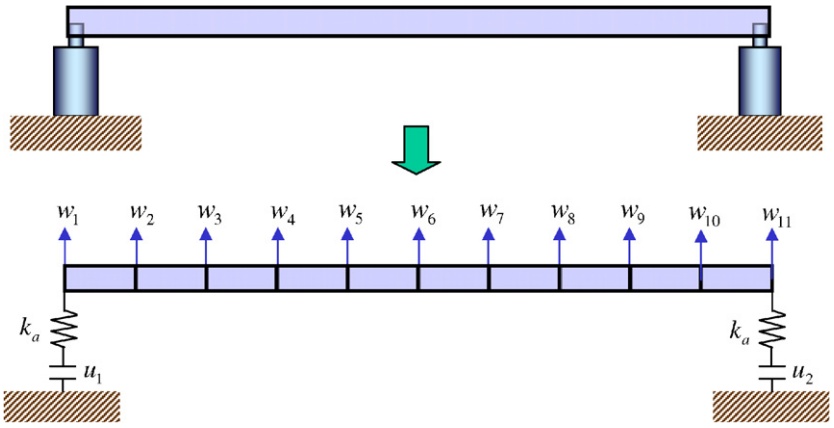

Fig. 20. Model of a beam and MSAs.

Table 2
Natural frequencies and damping ratios of the beam

Mode	Natural frequency (Hz)		Damping ratio (%)
	Experiment	FEA	Experiment
1	25.6	24.8	0.50
2	98.1	98.7	0.30
3	220.0	220.4	0.14
4	387.4	387.6	0.11

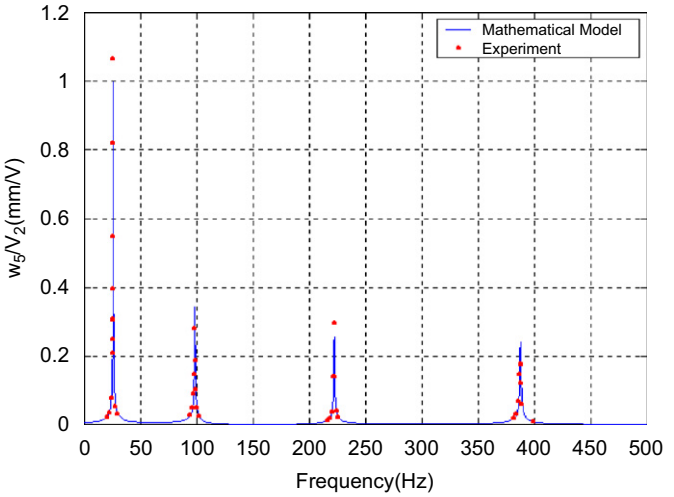

Fig. 21. Frequency response of normalized displacement at point w_5.

direction, only the symmetric modes are excited. In case of opposite direction, only the asymmetric modes are excited. Fig. 21 shows the transfer function at point w_5 when only one MSA is activated ($u_1 = u$, $u_2 = 0$ or $u_2 = u$, $u_1 = 0$). It means the MSA can control the dynamic response of the beam. Since the results are very good based on Table 2 and Fig. 21, the system matrices of the test structure are extracted well. Next, the total system including the beam, the MSA, and current amplifier is mathematically modeled to design the control logic. The MSA has linear dynamic characteristics and produces 9.17 μm/A driving current as addressed in

Sections 2 and 3. Since the homemade current amplifier is used to supply the working current to the MSA, the dynamics of the amplifier is included in the control logic. It is modeled by

$$\frac{I}{V} = \frac{b}{s+a}, \tag{15}$$

where $a = 439.82$, $b = 917.47$. The first four natural modes of the beam are considered to design the control logic. The reduced system matrices are obtained using the balanced model reduction method [13]. Finally, the controller is designed based on the well-known LQG method, and only one acceleration signal at w_5 point is fed back.

The performance of the designed control logic is tested using numerical simulation. When random excitation is loaded at point w_7, the displacement and acceleration responses at w_5 point are plotted in Fig. 22. Root mean square (rms) displacement is reduced to about 1/3 level, and rms acceleration to about 1/4 level. Since it is confirmed that the MSA and designed control logic have good control performance, the experimental tests are carried out. The tests are comprised of an impact test and a sinusoidal test. The impact test is conducted using an impact hammer. After the point w_7 of the beam is excited, the responses at point w_5 are measured. In the time domain, the measured acceleration response is plotted in Fig. 23. The impacted

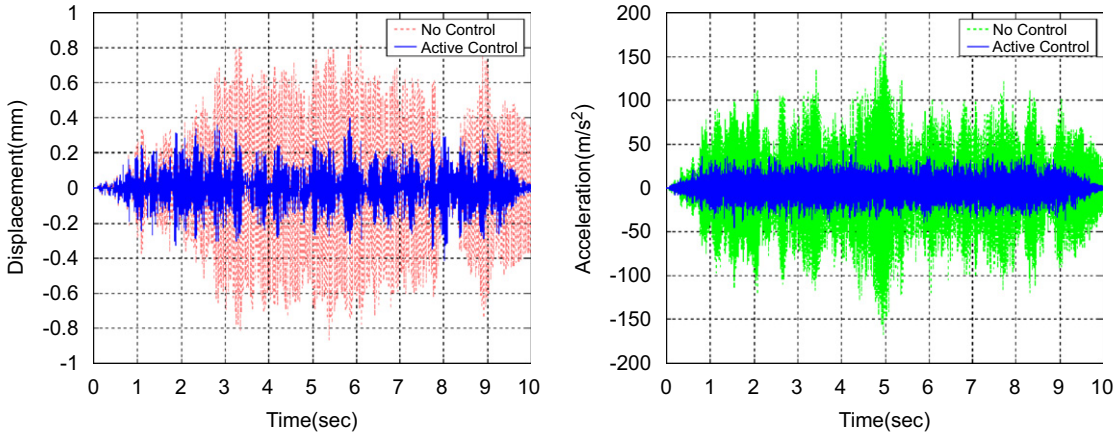

Fig. 22. Displacement and acceleration responses under random excitation.

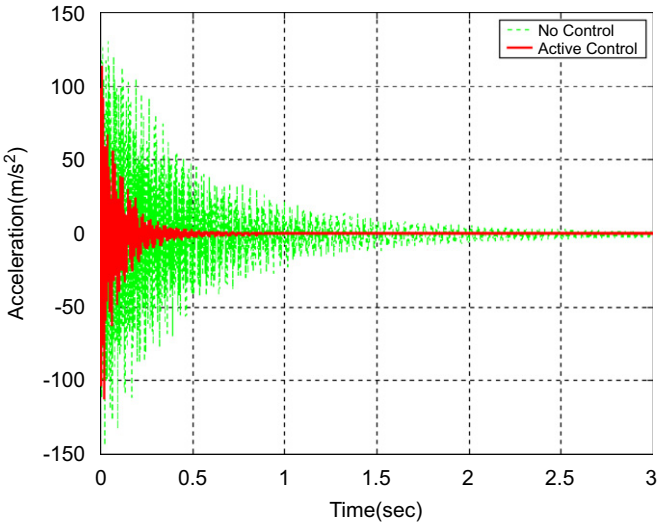

Fig. 23. Acceleration response under impact test (experiment).

response is sharply reduced by the active control. In the frequency domain, the transfer function of acceleration is shown in Fig. 24. The acceleration level is suppressed by about 15 dB at the 1st mode, 12 dB at the 2nd mode, 13 dB at the 3rd mode, and 20 dB at the 4th mode. In the sinusoidal test, one MSA is used as an exciter. The other is used as a control device. The beam is excited with constant frequency, which is each natural frequency of the beam. Of course, the responses at w_5 point are measured. Fig. 25 shows the measured displacement response at the fundamental natural frequency with and without control. To evaluate the control performance quantitatively, the reduction ratios obtained by active control are plotted using bar chart with respect to mode index in Fig. 26. The control system, including the MSA and control logic, can suppress the vibration level of the beam over 80%.

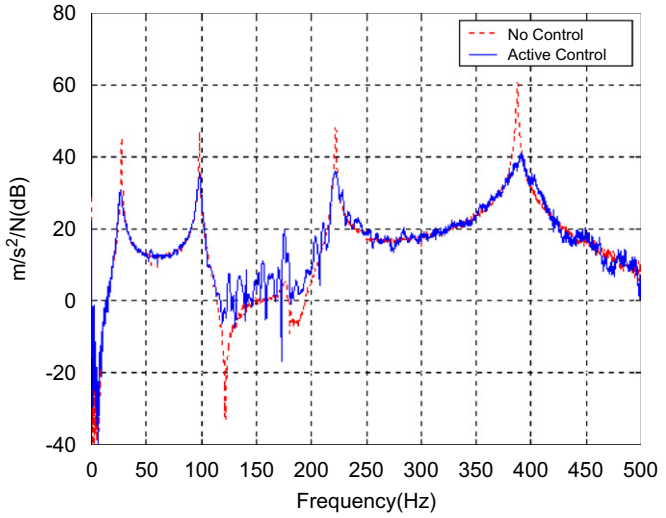

Fig. 24. Frequency response of acceleration under impact test (experiment).

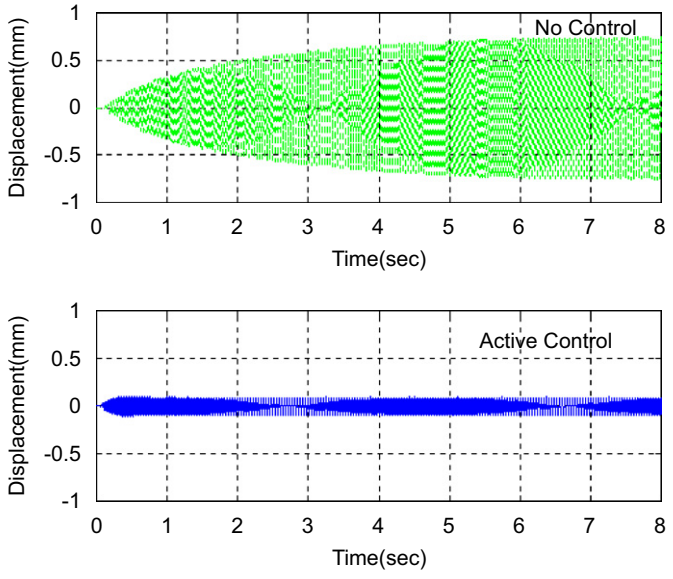

Fig. 25. Displacement response at the first natural frequency (experiment).

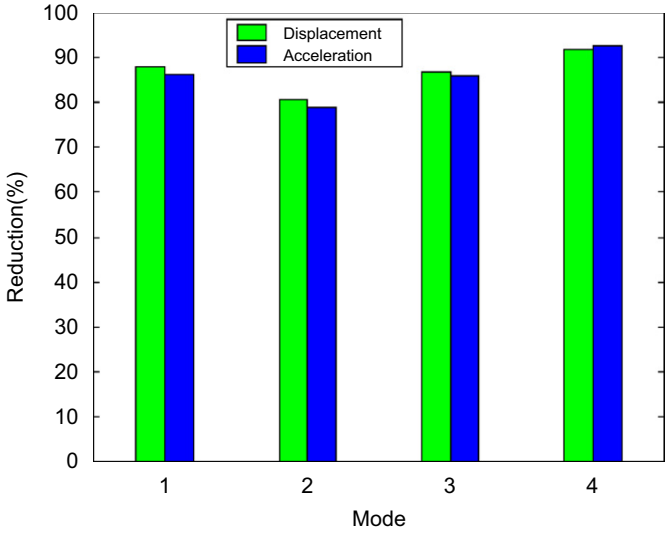

Fig. 26. Control performance of the MSA under sinusoidal excitation (experiment).

5. Summary

A MSA using Terfenol-D rod, measuring 25 mm in diameter and 100 mm in length, was designed and fabricated as a control device. The MSA consists of a Terfenol-D rod inside an electric coil for generating magnetic field and enclosed by an annular permanent magnet for magnetic bias. The Terfenol-D rod, the coil, and the magnet are assembled between two steel washers. The induced-strain actuator displacement can reach up to about 27 μm and the blocked force up to about 4000 N in the linear range. A series of experimental tests were performed to grasp the dynamic characteristics of the actuator, and they were then compared with theoretically obtained results. Induced-strain actuator displacements of the actuator measured by the test and predicted by magnetic analysis agreed well. Since it cannot be measured directly, the blocked force was estimated from the measurable parameters. The MSA was proved to have good linearity. A modeling method representing the exerting force of the actuator was confirmed through some testing results. The effectiveness of the MSA was explored as a control device. A series of numerical and experimental tests was carried out with a simple aluminum beam simply supported at each end by an actuator. After the equation of motion of the controlled system was obtained by the finite element method, a model reduction was performed to reduce the number of degrees of freedom. A linear quadratic feedback controller was implemented on a real-time digital control system to dampen the first four elastic modes of the beam. Although the linear MSA has small displacement amplitude, the control performance is satisfactorily reached. Therefore, it is confirmed that the linear MSA has good control performance and great capability as a control device.

Acknowledgments

The material is a part of the results of the research project sponsored by the Korean Ministry of Science & Technology as a National Research Laboratory project. This research is also financially supported in part by the Korean Ministry of Commerce, Industry and Energy as "Development of the Technologies on Ship Structural Safety Assessment and Noise/Vibration Reduction" project, by National Research Laboratory program (NRL:M10500000112-05J0000-11210), and by Brain Korea 21.

References

[1] M. Maertens, H. Waller, Vibration control of a plate structure with piezoelectric stack actuators, *Proceeding of the SPIE Conference on Smart Structures and Integrated System*, Newport Beach, March 1999, pp. 738–746.

[2] H.S. Tzou, Multifield transducers, devices, mechatronic systems, and structronic systems with smart materials, *The Shock and Vibration Digest* 30 (1998) 282–294.
[3] A.G. Jenner, R.J.E. Smith, A.J. Wilkinson, R.D. Greenough, Actuation and transduction by giant magnetostrictive alloys, *Mechatronics* 10 (2000) 457–466.
[4] K. Prajapati, R.D. Greenough, A. Wharton, Magnetic and magnetoelastic response of stress cycle Terfenol-D, *Journal of Applied Physics* 81 (1997) 5719–5721.
[5] E. Monaco, F. Franco, L. Lecce, Designing a magnetostrictive actuator by using simple predictive tools and experimental data, *Proceedings of the Seventh International Conference on New Actuators*, Bremen, August 2000.
[6] F. Stillesjo, G. Engdahl, C. May, H. Janocha, Design, manufacturing and experimental evaluation of a magnetostrictive actuator for active vibration control and damage analysis, *Proceedings of the Seventh International Conference on New Actuators*, Bremen, August 2000.
[7] A. Maier, W. Seemann, A note on the modeling of a magnetostrictive transducer, *Proceedings of the Third World Conference on Structural Control*, Como, May 2002, pp. 539–544.
[8] K. Schlacher, K. Zehetleitner, Magnetostrictive actuators for the control of smart structures, *Proceedings of the Third World Conference on Structural Control*, Como, May 2002, pp. 545–553.
[9] T. Zhang, C. Jiang, H. Zhang, H. Xu, Giant magnetostrictive actuators for active vibration control, *Smart Materials and Structures* 13 (2004) 437–477.
[10] ETREMA Products, Inc., 〈http://www.etrema-usa.com〉.
[11] G. Engdahl, *Handbook of Giant Magnetostrictive Materials*, Academy Press, San Diego, USA, 2000 (Chapter 3).
[12] V. Giurgiutiu, C.A. Rogers, Energy-based comparison of solid-state induced-strain actuators, *Journal of Intelligent Material Systems and Structures* 7 (1996) 4–14.
[13] K. Zhan, J.C. Doyle, *Essentials of Robust Control*, Prentice-Hall, USA, 1998 (Chapter 7).